Quantitative studies of nonlinear second sound in superfluid ^{4}He

Lori S. Goldner, Guenter Ahlers, and Ravi Mehrotra*
Department of Physics and Center for Nonlinear Sciences, University of California, Santa Barbara, California 93106
(Received 8 February 1990; revised manuscript received 4 February 1991)

Experimental studies of the nonlinear evolution in time of planar second-sound pulses in superfluid ^{4}He have been carried out at temperatures 2 to 25 mK below T_λ. The pulse evolution in helium is compared to solutions of the Burgers equation, and corrections for the effect of the heater and bolometer substrates are made by numerical integration of the heat-diffusion equation with appropriate boundary conditions. Agreement between measured and calculated pulse shapes is found to be excellent. Fits to the data of the model are used to obtain the linear second-sound velocity. A new method for studying the critical behavior of second sound very close to T_λ, where nonlinear effects are always important, is suggested.

I. INTRODUCTION

One of the great successes of two-fluid hydrodynamics[1] has been the prediction of the velocity u_2 and damping D_2 of second sound in terms of thermohydrodynamic parameters and transport coefficients.[2] Indeed, experimental determinations of these parameters have provided a detailed test of the theory. Most often, the theory has been used in a linearized form which is valid only for small-amplitude sound, and much of the effort that has gone into comparing experiment and theory has depended on the existence of a parameter range where the linear equations are a sufficiently good approximation for the amplitudes accessible in experiments. A more extensive test of two-fluid hydrodynamics involving the nonlinear terms is desirable, and several studies have been done. One of the earliest observations of the formation of shocks in second sound was reported by Osborne,[3] followed shortly thereafter by a measurement of the amplitude dependence of the velocity of second sound.[4] Since then, studies of second-sound propagation in a nonlinear regime have been used to probe various nonlinear aspects of the theory.[5–12] Much of this work pertains to parameters for which a nonlinearly propagating pulse has attained a self-similar shape involving a shock front.[5–7,9] Very little quantitative work has been done on the early-time evolution of second-sound pulses of given initial shape before the formation of a shock.[10] This early-time evolution is very sensitive to the nature of the nonlinear terms in the hydrodynamic equations and is the topic of this paper. The good agreement of our pulse-shape measurements with the theory provides a detailed experimental confirmation of the corresponding nonlinear terms in the two-fluid hydrodynamic equations.

Furthermore, an understanding of the effect of the nonlinear terms on the evolution of second-sound pulses allows us to extend the region over which we can measure certain critical properties of helium. For example, the determination of the superfluid density ρ_s is of great interest in the study of critical phenomena. Using the expression

$$u_{20}^2=\sigma^2\frac{\rho_s T}{\rho_n C_p}\ , \tag{1}$$

and measurements of the entropy per unit mass (σ), the heat capacity per unit mass (C_p), and the zero-amplitude limit of the second-sound velocity (u_{20}), the superfluid density can be determined.[13] In this expression, ρ_n is the normal-fluid density, such that $\rho_s+\rho_n=\rho$, the density of helium. Where nonlinearities can be ignored, the second-sound velocity u_2 is a good approximation to u_{20} and direct measurement of u_2 can be used to determine ρ_s. However, sufficiently near the superfluid transition temperature $T_\lambda(P)$, second sound of any measurable size propagates nonlinearly, and u_2 never approximates u_{20}. We describe a method for extracting u_{20} from second-sound pulse measurements in this region. The superfluid density can then be calculated from the linear expression [Eq. (1)], even in the region where linear second sound is not directly accessible.

It has been shown theoretically[14–16] that the normal-fluid velocity v_n in a second-sound planar pulse is given (to lowest nonlinear order) by solutions of Burgers equation. We show that one can account quantitatively for the measured time evolution of the shape of nonlinear planar second-sound pulses propagating in the fluid in terms of solutions of this equation.[17] For this purpose we have undertaken a detailed study of pulses at large enough amplitudes near enough to T_λ that nonlinear effects can be clearly seen, but far enough from T_λ so that the linear amplitude-range is also experimentally accessible. In practice, this meant working at temperatures from 2 to 25 mK below T_λ. In the quantitative comparison between the experiment and theory, we found it necessary to include careful thermal modeling of the pulse generator (heater) and detector (bolometer). Our composite model thus includes heat diffusion in the

heater and bolometer substrates, as well as propagation in the fluid as described by the Burgers equation. This model is applicable only to planar pulses for which the sound-propagation problem reduces to one with a single spatial dimension. In the design of our experiment, we have made considerable effort to assure that this condition is met.

In the region where we have tested our model, the velocity u_2 and the damping D_2 of second sound have been determined by other experiments.[18–21] We used the known values for D_2 in the model and performed a single-parameter fit to u_{20}. This parameter determines primarily the overall arrrival time of the pulses and has virtually no influence upon their shape. Our pulse shapes agree well with the model, even though the theory includes only the lowest-order nonlinearities and neglects coupling to first sound.

The damping, when it is at all important, has a significant influence on the *shape* of a nonlinear pulse because it primarily diminishes the strength of the high-frequency Fourier components which are generated by the nonlinear terms. The pulse shape thus is the result of the competition between the nonlinear terms and the damping when components of sufficiently high frequency are present for D_2 to play a role. Thus there is a parameter range over which D_2 can be determined with meaningful accuracy from the shape of the pulse. This is so because the strength of the nonlinear term[2] is known from independent thermodynamic measurements and need not be determined from this experiment. Since u_{20} determines primarily the overall arrival time of a pulse and not its shape, the correlation between u_{20} and D_2 is small, and both can be determined from a single experiment with meaningful accuracy, provided D_2 is sufficiently large to have an influence. If the model described herein remains valid very close to T_λ, we expect that pulse-shape measurements will yield values for D_2 in a region where conventional measurements are no longer able to give a meaningful value. If our model fails closer to T_λ, a more inclusive expansion of two-fluid hydrodynamics should still yield values for D_2.

Other studies by Worthington, Yan, and Trefny[22,23] have extracted second-sound velocities and attenuations from pulses at temperatures below 1.20 K. In their case it was not necessary to explicitly account for nonlinear effects, and extrapolations to zero input power were possible. Pulse modeling was used to account for three-dimensional and geometrical effects that are not present in the study described here.

In the next section of this paper, we describe various experimental aspects of this work. This is by far the longest section. It includes a description of our bolometers and their resolution for second-sound detection, a discussion of conditions for planar propagation, and a presentation of our procedure for dealing with various forms of pulse distortion. Our experimental procedure is also discussed in this section. In Sec. III we discuss the calculation of nonlinear pulse shapes from the Burgers equation and the thermodynamic information which is necessary for this purpose. Some results are represented in Sec. IV, and our conclusions are summarized in Sec. V.

II. EXPERIMENTAL TECHNIQUES

A. Overview and apparatus

The low-temperature apparatus consisted of two sealed sample cells of different lengths, filled through a capillary with ^{4}He and immersed in a bath of superfluid ^{4}He (Fig. 1; for clarity, only one cell is shown). Each cell contained a second-sound generator (in this case a large, planar heater) and a small, fast superconducting bolometer located on opposing walls. The cells were surrounded by a superconducting magnet, which was used to shift the transition temperatures of the bolometers to the desired range. A heat pulse launched at one wall of the cell travels back and forth in the cell and is detected each time as it reflects off the cell wall containing the bolometer. The bath temperature was regulated to better than 1-μK stability[24] using a five-wire germanium-thermometer bridge[25] and a 0.3-kΩ heater.

For our purposes the cell geometry is of great importance. The data will be compared with a one-dimensional version of the theory, and the cells were designed with this comparison in mind. The uniform planar heater extends over the entire lateral dimensions of the cell. We will detect one-dimensional pulses as long as signals from the edges of the heater or reflections at the walls have not yet reached the detector. From the placement of our heaters, bolometers, and cell walls, we expect that the first six reflections of the pulse at the bolometer in the

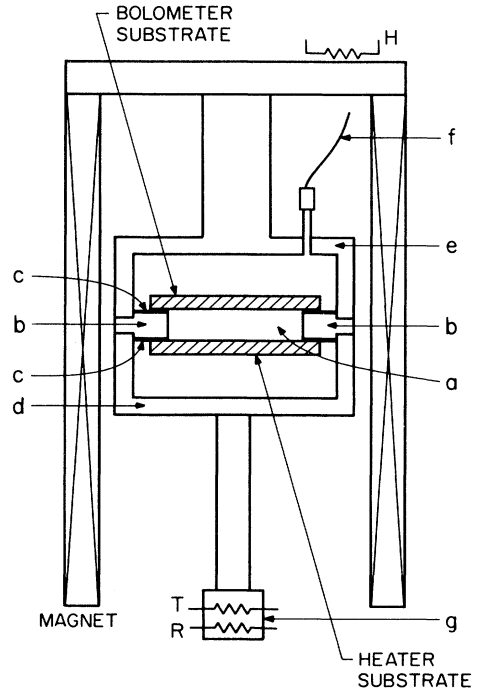

FIG. 1. Schematic diagram of the experimental apparatus. (a) Sample cell volume, (b) copper spacer, (c) Mylar spacers, (d) bottom copper cap, (e) top copper cap, (f) fill capillary, and (g) germanium thermometer (T) and reference resistor (R). H: heater.

short cell and the first two in the long cell will be free of three-dimensional effects.

The heater input was generated by a Wavetek model 178 programmable wave-form synthesizer, and a separate measurement directly detected the voltage at the heater. Thus the measured temperature amplitude, which depended on the bolometer calibration, could be checked against the known heat input. Digitizing of the voltage at the heater was accomplished through the use of a Nicolet model 12/70 signal processor to 8-bit accuracy.

Bolometers were biased with a constant dc current, and their voltage output was amplified using a PAR model 118 differential preamplifier and a PAR model 114 signal-conditioning amplifier. The output of the model 114 amplifier was also digitized by the signal processor, and some signal averaging was used to increase the signal-to-noise ratio.

B. Cell geometry

The geometry (Fig. 1) was defined by two flat Pyrex plates separated by a copper spacer [Fig. 1(b)] with a cavity of square (3.18×3.18 cm^2) horizontal cross section [Fig. 1(a)] in the middle. The thickness of this spacer, and therefore the length of the cavity, varied in the two cells. The heater, bolometer, and their respective electrodes were deposited on the inner surfaces of the Pyrex plates. In order to prevent electrical shorting of the electrodes by the copper spacer, Mylar spacers 51 or 127 μm thick [Fig. 1(c)] were inserted between the plates and the copper. At low temperatures the combination of Mylar and copper spacers were 0.362 cm thick in the one cell and 0.120 cm thick in the other, so that the long cell was about 3 times the length of the short cell, and both cells were quite broad and flat. Copper caps [Figs. 1(d) and 1(e)] covered both ends of the cell and were sealed to the copper spacer using gold O rings. Clearance holes were drilled in the copper spacer to allow for the bolometer and heater leads. Feedthroughs[26] for the heater and bolometer leads were epoxied into the copper caps.

In each cell the top copper cap contained a fill hole to which a short length of copper capillary was soldered. Small stainless-steel capillaries [Fig. 1(f)] with brass connectors silver soldered on were then soft soldered to the copper capillaries; a single 0.25-mm-i.d. stainless-steel capillary was used to fill both cells through a brass connecting T, and this capillary was sealed at the cryostat top with a valve.

C. Heaters

Each heater [Fig. 2(a)] consisted of a thin (approximately 200-Å) chromium film vapor deposited on a Pyrex 7740 substrate ($3.8\times3.8\times0.32$ cm^3). Thick (1500-Å) gold electrodes bordered two sides, and the chromium covered an open surface that was 3.18×3.18 cm^2 (so that it just filled the cell cavity). Their resistances at 2.1 K were 110.9 Ω in the short cell and 183.4 Ω in the long cell. The heater deposition was done using a line source[27] of length ≥ 2.54 cm and a source-to-substrate distance of 27 cm, ensuring that the heaters were uniform in thickness across their surface[28] to better than 2.5%.

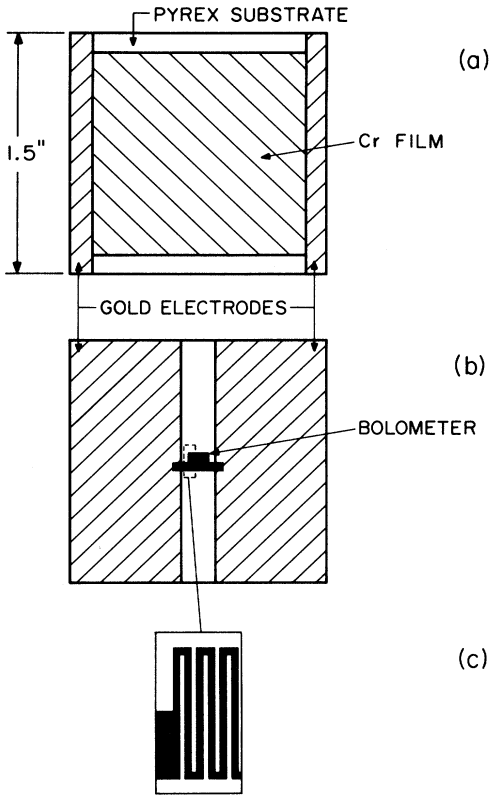

FIG. 2. Heater and bolometer on their respective substrates. (a) Heater, (b) bolometer, and (c) expanded view of bolometer trace. Not drawn to scale.

D. Bolometry

The bolometers [Figs. 2(b) and 2(c)] made fast detection of the sound pulses possible. Thin Pb-Au films[29] with zero-field superconducting transitions just above T_λ, similar to devices described elsewhere,[20,30–32] were made by a lift off procedure[33] to ensure maximum homogeneity of the films. Substrates were the same as for the heaters, and the source-to-substrate distance was again 27 cm, but the bolometers were much smaller, only 0.25 cm on a side. Electrodes were deposited first; then a photoresist pattern for the bolometer was placed on top of this, and gold (200 Å) and lead (430 Å) were deposited (in that order). Each bolometer was a single 42-μm-wide trace that folded back on itself 30 times [Fig. 2(c)] for a normal resistance just above the transition of 3500 Ω for bolometer 1 (in the long cell) and 4200 Ω for bolometer 2 (short cell). Room-temperature resistances were 17.4 and 19.3 kΩ, respectively.

A magnetic field ranging up to about 800 G was provided by a superconducting magnet in the persistent mode and was used to tune the transition into the desired temperature range. With the bolometer biased with a constant current, temperature fluctuations could be determined from changes in the voltage across it by using

$$\delta V = i\frac{dR}{dT}\delta T \ . \tag{2}$$

Here R is the bolometer resistance, i is the current through the bolometer, and δT is the incremental temperature change. A typical figure of merit, $K = R^{-1} dR/dT$, was about 60 K^{-1} at a resistance of 300 Ω and a bias current of 54 μA. Currents between 10 and 200 μA were employed.

Resistance-versus-temperature curves for bolometer 1 are shown in Fig. 3(a). Bolometer 2 is similar. Bolometer slope dR/dT versus resistance and figure of merit versus resistance are plotted in Figs. 3(b) and 3(c), respectively. Both were calibrated against a germanium thermometer at each field and temperature at which second-sound data were taken, immediately before or after measurements were completed. To accomplish this each device was biased at the working current and the voltage across it at different temperatures was measured with a Keithley model 195 or 196 multimeter. As can be seen from the figures, these devices are quite current sensitive, so that the addition of the *digital* multimeters to the circuit can cause both noise and a slight shift in the calibration. Nonetheless, the precision of these calibrations was about 0.1%, and the accuracy 1% or better. Typically, resistance measurements were taken at intervals of 4 mK for ±12 mK about the working temperature. Since regulating the open bath required always working below T_λ, smaller intervals were used closer to T_λ. Bolometer slopes and figures of merit were determined from this data using a spline fit.

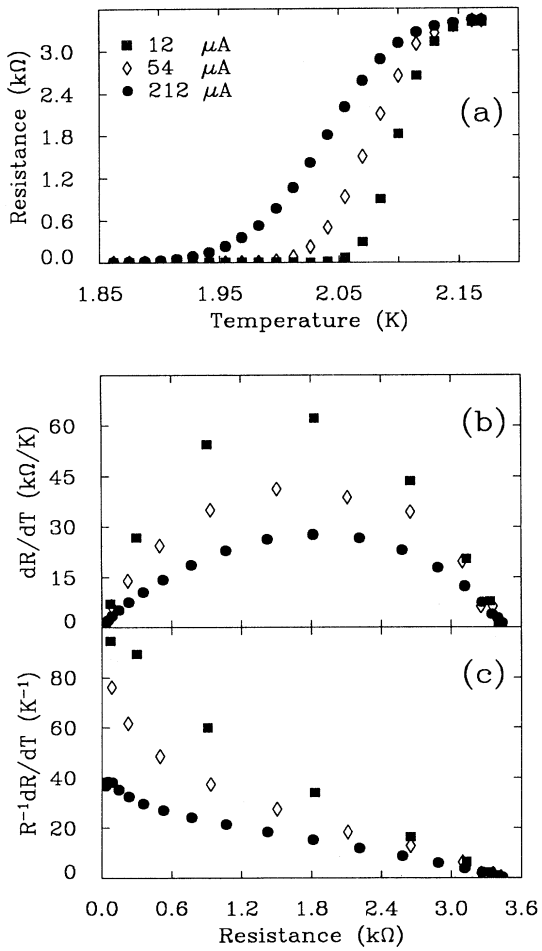

FIG. 3. Characteristic curves for bolometer 1 in the long cell. (a) Resistance vs temperature at various bias currents, (b) the bolometer slope (dR/dT) vs resistance, and (c) $R^{-1} dR/dT$ vs resistance.

E. Resolution

In theory (for biasing with a perfect current source), the resolution of these devices should be limited by Johnson noise voltage, which is given by[34]

$$\delta V_n = (4k_B TR\,\Delta f)^{1/2} . \tag{3}$$

With the typical values $K = 60$ K^{-1}, $R = 300$ Ω, $i = 50$ μA, and $\Delta f = 300$ kHz, Eqs. (2) and (3) give a resolution of 0.1 μK at 2 K. In practice, our resolution was about an order of magnitude worse than this because of an amplifier noise voltage of about 2.3 nV/$\sqrt{\text{Hz}}$, but some averaging over successive pulses brought it down again to the submicrokelvin region. For future work very near T_λ where much smaller sound amplitudes will have to be used but lower frequencies are sufficient, the use of a smaller bandwidth (say 30 kHz) and moderate signal averaging (of about 200 pulse sequences) will yield a resolution of 0.03 μK.

F. Thermometry and temperature regulation

A germanium thermometer in a five-wire bridge[25] arrangement was used to regulate the bath temperature to better than 1-μK stability.[24] Output from the bridge was fed back into a Linear Research model 130 temperature controller, the output of which drove a 301-Ω metal-film resistor in the bath space. The thermometer was calibrated against ^{4}He vapor pressure using the 1958 vapor pressure scale of temperatures.[35] Since the bolometers required working in a magnetic field, our thermometer was surrounded by a lead-foil tube to exclude the field and thus prevent drift.[36] Nonetheless, it was not used to determine absolute temperatures, but only for bolometer calibrations and bath regulation.

Absolute temperatures were determined for each data set from the second-sound velocity at vapor pressure using the data of Ref. 21. Errors were limited by the uncertainty in the cell lengths; an uncertainty of 7 μm in the length of the shorter cell leads to uncertainties in the temperature of only 150 μK at $T_\lambda - T = 0.01$ K.

G. Pulse distortion

The input to the heater from the Wavetek model 178 synthesizer is a voltage haversine, yielding a haversine squared for the heater power. However, even in the linear regime, the pulse measured at the bolometer (and, in fact, even the temperature pulse that leaves the heater) is not quite a haversine squared. Factors which contribute to pulse distortion can be minimized by working in appropriate frequency regimes, but nonetheless must be well understood in order to interpret the data.

1. *Thermal boundary effects*

Without the large Kapitza (thermal) resistance between the heater/bolometer substrates and the helium, this experiment would not be possible. It is only because of the large reflection coefficient at the walls of the cavity, which is due primarily to the Kapitza resistance, that detection of successive echoes is at all possible. A discussion of the second-sound attenuation at the walls and ends of the cavity can be found in Ref. 20. At the ends of the cavity (the bolometer and heater substrates), these losses are found to be negligible. The side-walls are irrelevant in our work since we never detect second sound reflected from these walls in this experiment (see Sec. II G 2 below).

While the Kapitza resistance prevents reflection losses once a pulse has been launched into the helium, it also delays and distorts the pulse launched at the heater and the pulse detected at the bolometer. For example, launching a pulse of peak power 10 mW/cm^2 heats up the substrate and causes a temperature jump up to 5 mK across the heater-helium boundary if the Kapitza resistance is 0.5 cm^2 K/W. This temperature jump is typically two orders of magnitude larger than the second-sound amplitude. It will lead to a temperature gradient and thus heat diffusion into the glass substrate away from the helium. After completion of the heater pulse, most of this heat diffuses slowly back toward the heater-helium boundary and will be released into the helium. While the net conductive heat loss through the glass is negligible, the distortion due to the combination of the boundary resistance and the thermal mass of the heater substrate is not. A similar situation prevails at the bolometer. While the heat loss into the bolometer substrate is negligible in its effect on the pulse in the helium (here the very large Kapitza resistance leads to a very small heat current into the bolometer), thermal gradients in the glass will again cause distortion of the detected pulse. We take both effects into consideration by numerically integrating the heat-diffusion equation with the following boundary conditions.[37]

At the heater the total heat flux j_0 as a function of time is given by the Joule heating corresponding to the heater voltage, and conservation of energy requires

$$j_0(t)=j_g(t)+j_h(t) , \tag{4}$$

where j_g is the heat flux into the glass substrate and j_h is the heat flux into the helium. At the bolometer the total heat flux is zero. We also have the jump condition at the boundary,

$$T_g-T_h=R_K j_h , \tag{5}$$

where T_g and T_h are the temperatures at the boundary in the glass (i.e., at the heater or bolometer) and helium, respectively, and R_K is the Kapitza resistance. Finally, at the boundary we use the linear relationship, for heat flow in the helium (in one dimension),

$$j_h=\rho C_p u_{20}(T_h-T_0) , \tag{6}$$

where u_{20} is the linear velocity of second sound, C_p is the heat capacity per unit mass at constant pressure of helium, T_0 is the unperturbed temperature of the system, and ρ is the density of helium. This expression can be derived from the linear relation $v_n=(T_h-T_0)u_{20}C_p/(\sigma T_0)$ and the boundary condition $j_h=\rho\sigma T_0 v_n$, where v_n is the velocity of the normal-fluid component, σ is the entropy per unit mass of helium, and where we have assumed that there is no net mass flow. It is important to note that we use this relationship only at the boundary, and not once the second sound has propagated any distance into the helium.

To complete this part of the model, we need the Kapitza resistance (R_K) of the heater-helium or bolometer-helium interface. In the analysis of the actual data, we use for the initial pulse the bolometer signal for the first echo and calculate the bolometer signal for the nth echo. This leads to cancellation of most of the thermal effects of the substrate and interface. To estimate a value for R_K, we used the power output measured at the heater as the initial condition. This pulse is modified slightly, but significantly, by the thermal boundary effects when it enters the helium. An additional effect occurs when the pulse is detected at the bolometer. As a result of the cumulative effects at the heater and bolometer, the effect of the Kapitza resistance is quite pronounced here. A value of 0.5 cm^2 K/W was consistent with the measurements in both cells, and this value was used in all fits shown in Figs. 7–9 below.

It is interesting to note here that Tsoi and Nemirovskii[38] (TN) have in fact suggested using nonlinear second sound as a probe of the Kapitza resistance. In their analysis of the heater-helium boundary, a characteristic relaxation time $\tau\approx R_K C_H$ for thermal energy transfer into the helium is deduced. Here C_H is the specific heat per unit area of the heater. After the onset of a square pulse at the heater, the amplitude of second sound into the helium will exponentially approach its maximum value with time constant τ. TN point out that the dependence of second-sound speed on amplitude, which is in turn dependent on $\tau(R_K)$, may be used as a probe of R_K. We note also that in their analysis, TN assume a thin planar heater so that the heat flux is given by $C_H\,\partial T_g/\partial t$. This simplification greatly enhances the tractability of the problem, but it cannot be used here because of the effect of the heater substrate.

Figure 4 shows an example of the effects of the boundaries on a heat pulse and detected signal. In Fig. 4(a) the measured heat flux at the heater $j_t(t)$ (open circles) and the calculated heat-flux profile in the helium $j_h(t)$ (solid line) are shown. The current $j_h(t)$ is then used as an initial condition for the solution of the Burgers equation in the helium (see Sec. III), which results in a temperature profile incident on the bolometer given by the open circles in Fig. 4(b). This incident pulse reflects almost perfectly from the bolometer substrate, so much so that the reflected pulse is indistinguishable in our measurements from the incident pulse. However, the small heat current that does enter the bolometer substrate gives us a temperature profile at the surface of the substrate (i.e., at the bolometer) that is given by the solid line in Fig. 4(b). Note that, as well as being slightly modified in

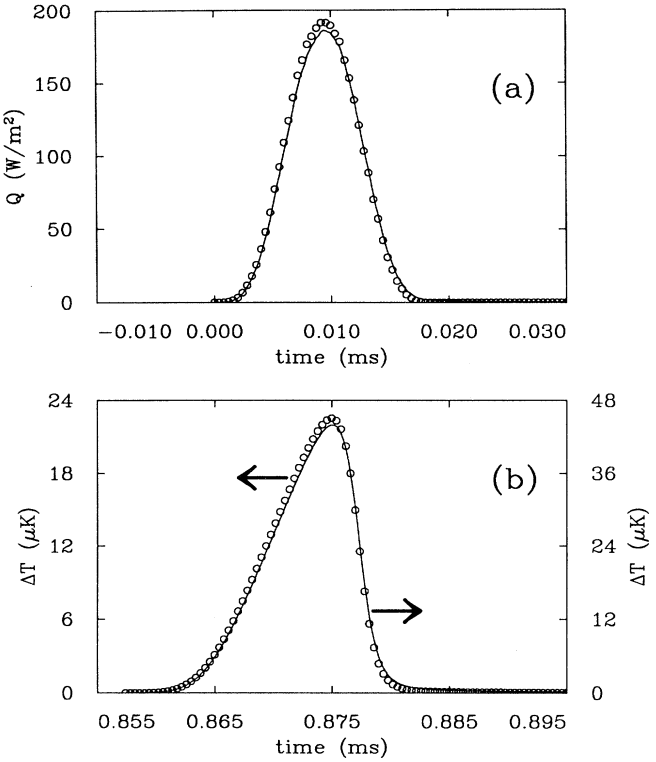

FIG. 4. Demonstration of thermal boundary modeling. (a) The open circles are the power per unit area measured at the heater, and the solid line is the calculated heat flux into the helium. (b) The open circles (left scale) represent the calculated temperature profile of the second-sound pulse incident on the bolometer, and the solid line (right scale) is the calculated temperature profile of the bolometer. Note the differently scaled ordinates. The reduced temperature t is 2×10^{-3}, and the cell length is 0.362 cm.

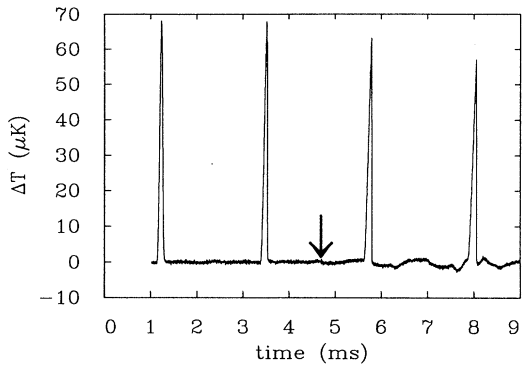

FIG. 5. First four pulse echoes in the long cell are shown. The arrow indicates when the first signals from the edge of the heater will reach the bolometer. Rarefactions are clearly seen after this time, indicative of three-dimensional effects. For these data, $t=10^{-3}$ and $u_{20}=322$ cm/s.

shape, the amplitude of this pulse is very close to twice that of the incident pulse, a consequence of the nearly perfectly reflecting boundary conditions. In this example the reduced temperature was 2.0×10^{-3} and the bolometer was 0.362 cm from the heater (long cell). The pulse is somewhat shorter in duration than those used in this study, in order that the thermal effects be more pronounced. Any work at even higher frequencies requires a better knowledge of R_K and the thermal properties of the glass.

For the heat capacity and the thermal conductivity of the glass, we used the values 0.03 J/(kg K) and 0.05 W/(m K), which have been measured[39] for Pyrex 7740. The heat capacity is somewhat dependent upon the magnetic field, making an accurate estimation difficult. The density of the glass[39,40] was taken to be 2.23 g/cm^3.

2. *Three-dimensional effects*

For spherical waves exclusively positive-going pulses as in Figs. 6–9 below are not possible, and rarefactions always follow a positive excursion. This is true for compressional waves[41] as well as waves of second sound.[7] Since the pulse input at the heater is necessarily a positive-going entropy wave, any negative-going excursions below the base line are clear evidence of three-dimensional effects. In our cells no such effects are observed until the time when second sound generated at the edges of the heater reaches the bolometer. This is illustrated in Fig. 5, where a typical data set for the long cell is shown. The first four echoes recorded at the bolometer are plotted, and the arrow indicates the smallest time of flight from a heater edge to a bolometer edge. A rarefaction begins to develop beyond that point, but until that time, the base line between pulses is flat to within the resolution of the experiment. The absence of rarefaction is also a confirmation that the heater uniformity is quite good; a nonuniform heater would cause the appearance of three-dimensional effects.

3. *Pulse interactions*

Pulses interact with themselves upon reflecting from the heater or bolometer substrate. Whereas this plays no role for linear pulses where superposition applies, it will in principle lead to pulse distortion for nonlinear (finite amplitude) pulses. Explicitly accounting for these interactions considerably complicates the analysis, and we have not done so. Instead, we take two different experimental approaches to show that this effect is negligible in our parameter range.

First, we measured second-sound pulses in two separate cells, one long and one short. Heat pulses of the same length and approximately the same amplitude were launched at the same temperature, and the resulting echoes were measured. The second arrival of the pulse in the short cell travels about the same distance as the first arrival in the long cell, except that in the long cell the pulse has undergone only one self-interaction (as it is detected) and in the short cell it has undergone three (bolometer, heater, and bolometer). Similar signals were run in both cells at all temperatures and pulse lengths, and no systematic differences were found between the pulse shapes. Since amplitudes in the two cells were

different by about 10%, no *direct* comparison of data in the two cells is possible. However, fits of the model described in Sec. III (which neglects these interactions) to the data were just as good and yielded the same results in both cells.

Even in a single cell, it is possible to probe the effects of self-interactions. If we launch a two-cycle haversine at the heater, the bolometer will detect first a pulse that has passed only through the reflected part of itself and then a pulse that has passed through both itself and the first pulse. Double pulses were run in the long cell at reduced temperatures of 10^{-3} and 2×10^{-3} and at single-pulse lengths [full width at half maximum (FWHM) of the initial pulse] as long as $\frac{1}{8}$ the cell length (or $\frac{1}{3}$ the cell length from start to finish). This is a region of parameters where nonlinear effects are relatively large and where the pulse spends a significant fraction of its time self-interacting. An example is shown in Fig. 6. Here each pulse has a FWHM of 0.022 cm, about 6% the length of the long cell (in which this set was taken), although its length from start to finish is 0.060 cm (about 16% of the length of the long cell). The data are taken at 10^{-3} in reduced temperature, the most nonlinear regime investigated ($\alpha=-126$; see Sec. III). Figure 6(a) shows the actual data for the first arrival of the pulse pair. For Fig. 6(b) we have shifted the second pulse along the time axis to coincide with the first using a least-squares algorithm and then plotted the two pulses and their differences [Fig. 6(c)].[42] The differences are a subtraction of the shifted second pulse from the first. Clearly, the agreement between the two pulses is excellent, and self-interaction does not play a significant role. Longer and shorter pulses were also used, but the nonlinear effects were less pronounced for the longer ones, and although nonlinear effects were more pronounced for the shorter ones, they self-interacted for relatively shorter periods of time. In all cases residuals were similar to those shown.

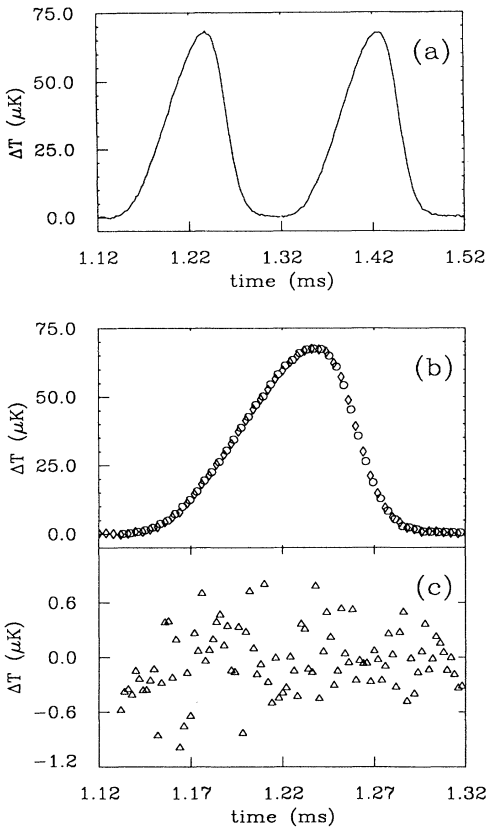

FIG. 6. Absence of distortion due to pulse interaction is demonstrated. For these data, $t=10^{-3}$ $\alpha=-126$, and FWHM $=0.022$ cm. Data were taken in the long cell, $l=0.362$ cm. (a) Raw data at the first arrival of a double pulse. (b) Open diamonds: first cycle; open circles: second cycle, time shifted so as to give a best fit with the first cycle. For clarity, only every other point is shown. (c) The difference between the first cycle and the time-shifted second cycle. All points are shown.

For the purposes of analysis of single pulses, we will use pulse lengths as small as or smaller than those shown in Fig. 6 (less than 6% the length of the long cell) so that the effects of self-interactions are negligible.

4. *Wedging*

The effect of a small angle between the heater and bolometer can be calculated for our square detector.[43] A slight wedge will cause the measured amplitude of a monochromatic plane wave reflecting off the cell end walls to be modulated by a function dependent on the geometry of the detector and phase variations across it. For the square detectors used here, we find that the envelope function by which a Fourier component of wave number k must be multiplied is

$$F(\theta,\alpha,k)=\frac{\sin[(n-\frac{1}{2})ka\theta\cos\alpha]}{(n-\frac{1}{2})ka\theta\cos\alpha}\,\frac{\sin[(n-\frac{1}{2})ka\theta\sin\alpha]}{(n-\frac{1}{2})ka\theta\sin\alpha},$$

for the nth arrival of the pulse at the detector (nth echo), where a is the size of a side of the detector (0.25 cm) and θ is the wedge angle. α is the angle between one edge of the detector and the plane formed by the incident and reflected wave vector of the pulse (plane of reflection). Note that if this angle is zero, the modulation function reduces to the form $\sin x/x$, where $x=(n-\frac{1}{2})ka\theta$. In this case phase variations are zero as we move across the detector parallel to one edge, and the plane of reflection is parallel to the other edge.

To estimate the size of any wedge in the apparatus described above, consider that the copper spacers used to separate the Pyrex substrates were flat and parallel to better than 5 μm. The Mylar spacers probably represent the largest source of alignment errors. Even for a total deviation from parallelism of 13 μm (roughly 10% of the thickest Mylar spacer) across the cell, θ would be only about 4×10^{-4} rad. This causes amplitude modulations of less than 4% for all wave numbers below 3100 cm^{-1} (wavelengths above 20.3 μm) provided only the first two echoes are considered; for wave numbers below 1570 cm^{-1} (wavelengths above 40.0 μm), this criterion holds for at least the first three echoes. In this study we restrict ourselves to pulses where significant Fourier components are not amplitude modulated by more than 4% as calculated using the above assumptions, which are probably

more restrictive than necessary. Furthermore, for the second-sound velocities relevant to this experiment, the frequencies corresponding to these wave vectors are sufficiently high that we avoid them anyway for electronic reasons.

5. *Electronics*

Finally, we consider distortion from electronic sources. In our case the largest effect was from a 300-kHz single-pole filter in line with the preamplifier for the bolometer circuit. This was deliberately installed to limit the noise bandwidth. In general, we tried to avoid working in a regime where this filter had a significant effect. However, where necessary, the effect of the filter could be accounted for in the modeling. Several more troublesome but even smaller effects remained.

The worst unaccounted signal distortion was due to the limitations of the preamplifier. Above 1 MHz, its gain fell off rather sharply. Small but noticeable phase shifts appeared even at much lower frequencies and led to distortions of the pulse shape. These effects, although small, nonetheless prevent accurate measurements of second-sound damping in this experiment. Shorter pulses with higher-frequency components would have been necessary for this purpose since we are working at or near the minimum in the second-sound damping (10^{-2}–10^{-3} in reduced temperature).

Each bolometer was connected to the room-temperature electronics through a shielded twisted pair of leads (Microtech MS-2) with a capacitance $C \lesssim 200$ pF. The simplest model for our bolometer circuit gives a single-pole cutoff frequency ω_c of $1/RC$ (where R is the bolometer resistance). In order to keep the bandwidth of our circuit as wide as possible, the bolometer was run at about 300 Ω, so that $\omega_c/2\pi$ was approximately 2.5 MHz. Working at low R lowered the bolometer sensitivity somewhat [see Fig. 3 and Eq. (2)], but gained enough bandwidth that any filtering effects from the cables were completely negligible.

In general, we worked at frequencies that were as small as possible and still fulfilled the requirements of Sec. II G 3; i.e., pulses had to be long enough not to contain or develop significant frequency components higher than 100 kHz and short enough that self-interactions were not noticeable.

H. Procedure

With the cells at about 4 K, helium was admitted to them through two liquid-nitrogen-cooled charcoal traps until the sample pressure was several atmospheres. The cells were then sealed and cooled to the working temperature. Helium contracts enough between 4 and 2 K that a liquid-vapor interface formed somewhere above the bolometer and in the top cell. Thus the sample was always at vapor pressure. A Texas Instruments model 149 pressure gauge was used to confirm the sample pressure.

In a typical experiment a single haversine voltage pulse was applied to the heater from the Wavetek model 178 function synthesizer, and the first several echoes of the resulting second-sound pulse at the bolometer were recorded and digitized with the Nicolet model 12/70 signal processor. Approximately 1 s later, after the sample returned to equilibrium, a second pulse was launched, and its first several echoes recorded and added to the previous signal. The signal input to the heater was also monitored and recorded. With all the timing controlled by an IBM PC/XT computer, this procedure was repeated anywhere from 1 to 100 times. Most data sets were the addition of about 30 such signals. Once complete, data sets were transferred from the signal processor to the computer over a serial port.

Our ability to use signal averaging depended strongly on our temperature stability. Fluctuations in temperature cause fluctuations in the second-sound velocity, meaning that successive pulses arrive at the bolometer at slightly different times. To ensure that signal averaging was not distorting the data, occasional single-sweep sets were taken several seconds to a minute apart. The results of two such sweeps were then subtracted. In general, residuals could be completely accounted for by noise in the pulse-shape measurement, and no evidence of systematic deviations could be found. For the smallest reduced temperatures and the shortest pulses (where the nonlinearites were most evident and shock fronts developed), signal averaging could not be done. However, these pulses were outside the range of this study (see previous section).

Bolometer calibrations (resistance R versus temperature T) were obtained every time the working temperature or magnetic field was changed. The bolometer resistance was measured immediately before or after each data set so that the slope dR/dT could be determined separately for each data set from the calibration and the known resistance.

As discussed in Sec. II G 1, it is possible to use the power applied to the heater as a boundary condition to solve for the initial heat pulse into the helium. From this and the nonlinear theory discussed in the next section, we can then calculate the pulse at the bolometer at the arrival times of successive echoes. Then the bolometer response can be modeled (including here the effect of electronic filtering) so that a direct comparison of the calculated and measured pulses is possible. However, as we also noted in Sec. II G 1, this procedure is quite sensitive to the characteristics of the substrate (R_K, the specific heat, and the thermal conductivities of the glass) as well as the second-sound velocity. So while we use this method to find a suitable value for R_K, we turn to a slightly different method for exploring the nonlinear properties of the fluid.

For our initial conditions we used the measured temperature profile of the first arrival of a pulse at the bolometer. Using this pulse for boundary values, we solved for the second-sound pulse that must have been reflected from the bolometer substrate. This reflected pulse then becomes the initial condition to solve for the temperature profile at the bolometer at the arrival time of the successive pulses. Then the bolometer response is modeled and a comparison with (or a fit to) the measured data is done. Here the fits are quite insensitive to the boundary parameters, and a single-parameter fit, adjusting only the linear second-sound velocity u_{20}, is used. In effect, since we are

starting and ending with a bolometer signal, most of the intermediate distortion at the boundaries cancels, as opposed to the method previously described and illustrated in Fig. 4 where the boundary corrections twice distort the initial signal and there is no cancellation.

Our model then consisted of three parts: a calculation at the bolometer boundary of the reflected pulse into the helium, a nonlinear calculation of the second-sound propagation in the helium, and another calculation at the bolometer boundary to account for bolometer response. The first and third of these have been discussed in Sec. II G 1. They are very nearly the same calculations; in the first case the temperature of the boundary is measured and the resulting reflected second-sound pulse is calculated, while in the third case the incident second-sound pulse is given and the boundary temperature is calculated. A Crank-Nicholson[44] method is used to numerically solve the diffusion equation in the glass. The nonlinear calculation of the sound propagation remains to be discussed.

III. CALCULATION OF NONLINEAR SECOND-SOUND PROPAGATION

If the equations of two-fluid hydrodynamics are expanded to second order for small changes in temperature (T) and small counterflow velocities, and if thermal expansion (i.e., the coupling to first sound) is ignored, it can be shown that the Burgers equation with damping describes the one-dimensional propagation of second sound.[14–16] In terms of the normal-fluid velocity v_n, the sound-pulse evolution is given by solutions of

$$\frac{\partial v_n}{\partial t}=\frac{D_2}{2}\frac{\partial^2 v_n}{\partial x^2}+(u_{20}+\alpha v_n)\frac{\partial v_n}{\partial x}\ , \tag{7}$$

where D_2 is the second-sound damping, u_{20} is the velocity of linear second sound given by Eq. (1), and α is the Khalatnikov nonlinear coefficient[2]

$$\alpha=\frac{\sigma T}{C_p}\frac{\partial}{\partial T}\ln\left[\frac{u_{20}^3 C_p}{T}\right]\ . \tag{8}$$

Here σ and C_p are the entropy per unit mass and heat capacity per unit mass at constant pressure of helium, respectively. Near T_λ, $\alpha\sim t^{-1}$ [where $t\equiv(T_\lambda-T)/T_\lambda$], so that the nonlinearities will be apparent even for the smallest amplitudes of v_n if t is small enough.

To calculate α we used entropy data from Ref. 25. The derivative $\partial u_{20}/\partial T$ was determined from a spline fit to the data of Ref. 21, and C_p [in J/mol K] was determined from the formula[45]

$$C_p=-A_0\ln t+B_0-D_0 t\ln t-E_0 t\ ,$$

where $A_0=5.100$, $B_0=15.52$ $D_0=-14.5$, and $E_0=69$. The second-sound damping (D_2) was taken from Ref. 20.

Burgers' equation is expected to describe the evolution of one-dimensional second sound in the regime where $(\delta\rho_s/\rho_s)\ll 1$ and where coupling to first sound is negligible. Furthermore, Burgers' equation describes only second sound traveling in one direction; it cannot account for interactions of left- and right-going pulses, for example, or for the interaction of a single pulse with itself as it reflects off a wall. We have shown experimentally that these self-interaction effects are unmeasurably small in the parameter range covered by this study. To lowest order the coupling of second to first sound may be neglected when $(C_p/C_v-1)\ll 1$. For helium at saturated vapor pressure, $(C_p/C_v-1)\leq 10^{-2}$ and these effects are small. The nonlinear coupling of first and second sound is discussed in a paper by Putterman and Garrett.[46] Some preliminary calculations indicate that the effect of this coupling is quite small, but further work is warranted, especially if the technique described herein is to be extended nearer to T_λ.

A qualitative understanding of the solutions of the Burgers equation is useful to understanding this experiment. If we set α equal to zero, we have a linear equation that describes the propagation of waves with speed u_{20} in one direction. For nonzero α the term in parentheses in Eq. (7) is an effective second-sound velocity u_2 for sound of amplitude v_n. Since α is negative near T_λ, larger-amplitude sound moves relatively slower, causing smooth pulses to lean backwards and eventually form shock tails. As higher wave numbers are generated by this steepening of the pulse shape, the damping term, whose strength increases with the curvature of the sound pulse, will have relatively larger effects on the shape of the pulse. Thus the competition between nonlinear steepening and linear dissipation determines the final shape of these pulses. Since α is known from thermodynamic measurements, pulse shapes can be used to determine the value of D_2.

For the present we hope to demonstrate that Eq. (7) in fact describes the evolution in time of second sound quite accurately, using previously measured values for D_2.

For numerically solving the Burgers equation, we again used a Crank-Nicholson scheme.[44] For this calculation we transformed into a frame moving with velocity u_{20}. This greatly simplifies the numerical work since all changes in second-sound amplitudes are relatively slow and due only to the nonlinear and damping terms. To implement this procedure, it was necessary to use the generated or reflected pulse shape (with appropriate thermal modeling) as an "initial" condition for the solution of the Burgers equation. Strictly, one should do the integration in a stationary frame and generate the pulse from the boundary condition at one wall. This procedure is much more demanding on computer time since very small spatial and time steps are required. We have carried it out for a few typical cases and compared it with the initial-value calculation in the moving frame. In the regime discussed in this study, there was no significant difference in the results obtained by the two methods.

IV. RESULTS

Typical examples of measured pulse shapes and fits of the model to them are shown in Figs. 7–9. All fits shown here used the first arrival of the pulse at the bolometer (a) as the initial condition and then fit u_{20} to the sixth echo (d). Parts (b) and (c) of these figures are comparisons of the model with echoes 2 and 4. In parts (b)–(d) the data

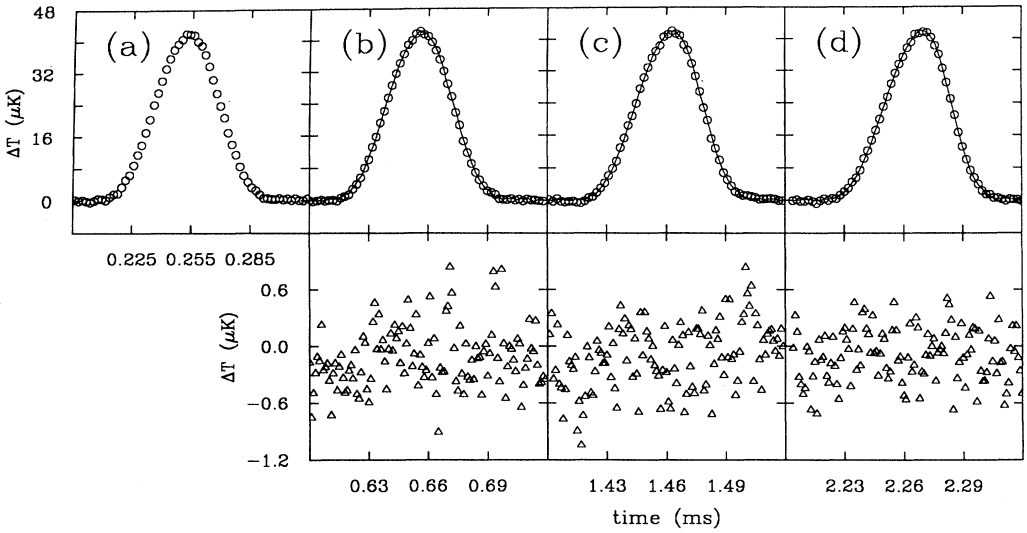

FIG. 7. Pulse evolution for $\alpha=-30.3$, $t=5.01\times10^{-3}$, $u_{20}=598.3$ cm/s, and $D_2=3.03\times10^{-4}$ cm^2/s. The FWHM of the initial pulse is 0.022 cm. (a) First echo, used to generate initial condition for the model. (b) Open circles: second echo; line: model. (c) Same as (b), but for fourth echo. (d) Same as (b), but for sixth echo. This echo was used to determine u_{20}. Residuals are shown below.

are plotted as open circles, and the fit is given as a continuous line. The residuals are plotted below each part. For clarity, not all data are shown; however, all residuals are plotted. Only data from the short cell are shown since more pulses are available for comparisons (recall that the first six are planar). Agreement of data obtained in the long cell with the model is equally good in all cases.

For Figs. 7 and 8 the theory and data are indistinguishable. In Fig. 9, which is at the same temperature as Fig. 8, but uses a shorter pulse, there is a very small discrepancy visible in the last echo, and the fit has a χ^2 per degree of freedom of 1.4. The data for the sharpening edge of the pulse here is slightly less steep than the model predicts; however, the difference is small enough that numerical errors, uncertainties in the values for the thermal properties of the glass or boundaries, or electronic filtering effects (all of which are more important at the higher frequencies present in this pulse) may well account for the entire effect (see Secs. III and II G 5). No discrepancies larger than those shown in Fig. 9 were found within the scope of this study.

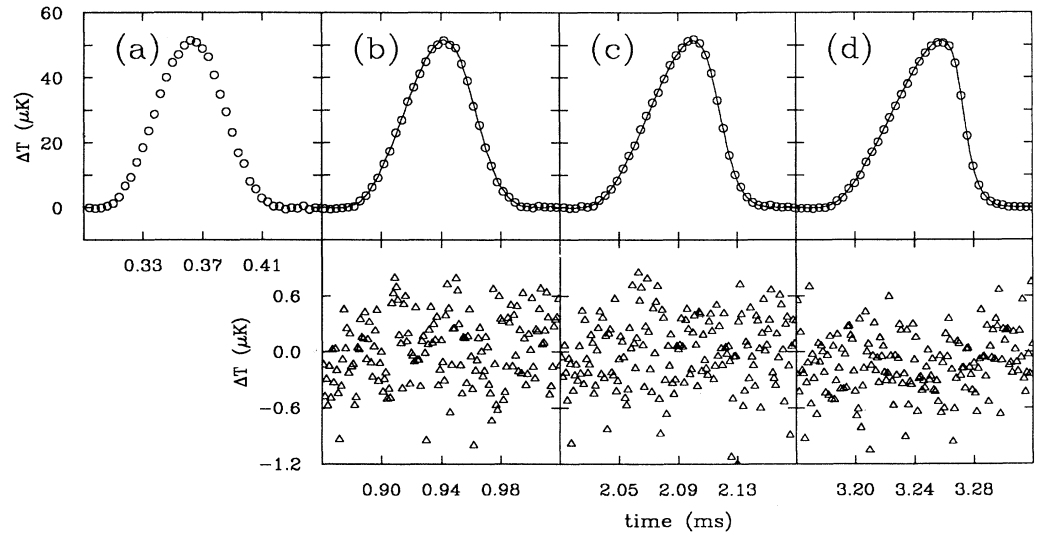

FIG. 8. Pulse evolution for $\alpha=-69.6$, $t=2.02\times10^{-3}$, $u_{20}=418.4$ cm/s, and $D_2=3.24\times10^{-4}$ cm^2/s. The FWHM of the initial pulse is 0.022 cm (a)–(d) are the same as for Fig. 7, except that, for clarity, only every fourth point is plotted. All residuals are plotted.

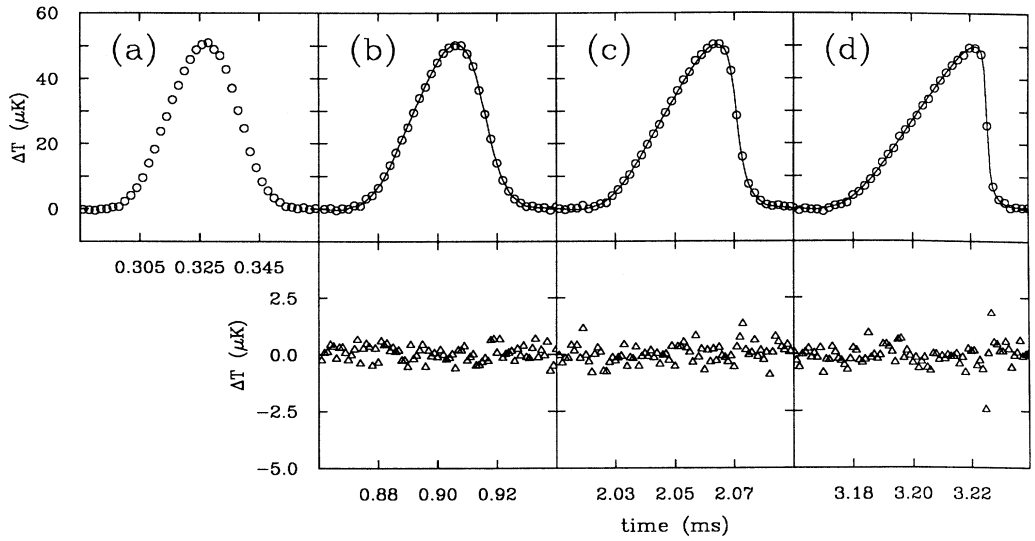

FIG. 9. Same parameters as Fig. 8, but the initial pulse FWHM is 0.011 cm. (a)–(d) are the same as for Fig. 8, except that every other point is plotted. All residuals are shown.

Since our model for the evolution of pulses in this system is based on the Burgers equation, any comparisons are subject to the restrictions discussed in Sec. III; for example, no coupling to first sound has been considered, and self-interactions of the pulse at the heater and bolometer substrates have been ignored. The requirement that $\delta\rho_s/\rho_s \ll 1$ is easily satisfied in all cases; typical second-sound temperature excursions are 60 μK or less, so that even at $t=1\times10^{-3}$, the smallest reduced temperature used in this study, $\delta\rho_s/\rho_s$ was only about 0.02. That the pulses we study are one-dimensional is discussed in the experimental section. Self-interactions are also discussed there, and the only experimentally untested assumption we make is that coupling to first sound is negligible.

All data and fits shown represent the temperature variations of the bolometer, rather than the second-sound temperature deviations. As discussed earlier, these pulse profiles are very close to a factor of 2 bigger and slightly modified from the profiles in the helium.

It is worth noting that while the fits shown were quite insensitive to the value of D_2, at only slightly shorter pulse lengths (involving slightly larger wave numbers), the sensitivity increased significantly. In the former case attempts to adjust D_2 led to errors about as big as or bigger than D_2 itself, while for the latter (at pulse lengths only a factor of 2 smaller) precision of the fits was about 10% of D_2. Unfortunately, because of the electronic distortions at high frequencies, the accuracy of these measurements is in doubt. So, in this study, we have confined ourselves to a regime where nonlinear effects are determining pulse shape, and dissipative effects are still quite small. However, closer to T_λ where both nonlinear and dissipative effects are larger, these pulse shapes should be considerably more sensitive to the value of D_2 at longer widths (lower wave numbers). We considered a pulse generated from a single cycle of a 10-kHz-voltage haversine applied at the heater at a reduced temperature of 10^{-5}. The initial FWHM of the pulse in the helium was 0.001 97 cm, corresponding to a width in time of 0.036 ms ($u_{20}\cong 54$ cm/s). Using our model, we calculate the shape of this pulse after one trip across the short cell. The results for two second-sound dampings, different by 20%, are shown in Fig. 10. Note that these pulses have a FWHM after a single pass across the short cell that is significantly longer than the initial FWHM. The initial amplitude, which was 1 μK, has also been significantly reduced. Only a slight sharpening of the pulse is visible as the increased damping effectively begins to cut off high frequencies generated by the nonlinear terms. The pulse, however, is far from linear; α is nearly -9000.

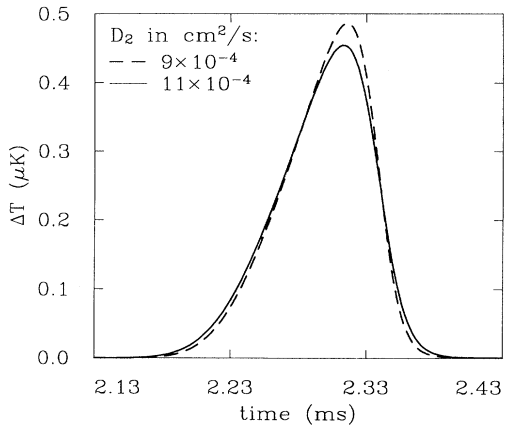

FIG. 10. Example of predicted second-sound pulse shapes at $t=10^{-5}$. For an initial condition, a single cycle of a 10-kHz haversine squared with peak input power 1.5 W/m^2 was used. The calculated temperature profiles in the helium at the bolometer (one flight time later in the short cell) with two different values for D_2 are shown.

V. CONCLUSIONS

In summary, we find good agreement of our data with solutions of the Burgers equation for temperatures from 2.2 to 22 mK below T_λ. The model takes into account the pulse distortion due to thermal effects in the detector, and in slightly modified form, it can also be used to model the second-sound generator and account for electronic filtering effects. The geometry of our experiment simplifies the problem, enabling us to use a one-dimensional theory and to disregard boundary effects at the copper-cell sidewalls. So far, coupling to first-sound and self-interaction effects have been ignored; however, such corrections may become necessary for work closer to T_λ, and further analysis in this regime may be needed.

The only adjustable parameter in this study has been the second-sound velocity, although it is possible to work in a region where there will be good sensitivity to the second-sound damping as well. Since pulse-shape measurements do not depend upon the linearity of the sound, it should be possible to extend or improve upon measurements of the second-sound damping and velocity[19,20,47] very near T_λ.

ACKNOWLEDGMENTS

We thank D. S. Cannell and P. K. Hansma for helpful and stimulating discussions. We are grateful to V. Steinberg for his participation in the early stages of this project and for the theoretical guidance which he has provided. This work was supported by National Science Foundation Grants Nos. DMR 84-14804 and DMR 89-18393.

*Present address: National Physical Laboratory, Dr. K. S. Krishnan Road, New Delhi 110012, India.

[1]L. D. Landau, J. Phys. USSR **5**, 71 (1941) [English translation: *Collected Papers of L. D. Landau*, edited by D. ter Haar (Gordon and Breach, New York, 1965), p. 301].

[2]I. M. Khalatnikov, *An Introduction to the Theory of Superfluidity* (Benjamin, New York, 1965).

[3]D. V. Osborne, Proc. Phys. Soc. London A **64**, 114 (1951).

[4]A. J. Dessler and W. M. Fairbank, Phys. Rev. **104**, 6 (1956).

[5]T. N. Turner, Physica **107B**, 701 (1981).

[6]J. C. Cummings, D. W. Schmidt, and W. J. Wagner, Phys. Fluids **21**, 713 (1978).

[7]L. P. Mezhov-Deglin, A. Yu. Iznankin, and V. P. Mineev, Pis'ma Zh. Eksp. Teor. Fiz. **32**, 217 (1980) [JETP Lett. **32**, 199 (1980)].

[8]M. O. Lutset, S.K. Nemirovskii, and A. N. Tsoi, Zh. Eksp. Teor. Fiz. **81**, 249 (1981) [Sov. Phys.—JETP **54**, 127 (1981)].

[9]A. Yu. Iznankin and L. P. Mezhov-Deglin, Zh. Eksp. Teor. Fiz. **84**, 1378 (1983) [Sov. Phys.—JETP **57**, 801 (1983)].

[10]W. Fiszdon, Z. Peradzynski, and G. Stamm, Phys. Fluids A **1**, 881 (1989).

[11]H. W. Liepmann and G. A. Laguna, Annu. Rev. Fluid Mech. **16**, 139 (1984).

[12]R. J. Atkin and N. Fox, J. Phys. C **16**, 1615 (1983).

[13]Here we neglect terms of order $(u_{20}/u_{10})^2$, which are always much less than 0.1%.

[14]S. Kitabatake and Y. Sawada, J. Phys. Soc. Jpn. **45**, 345 (1978).

[15]V. Steinberg (private communication).

[16]S. K. Nemirovskii, as quoted in Ref. 8.

[17]Very recently, solutions to this equation were compared with experimental results for the time evolution of the amplitude of cylindrical second sound by Fiszdon, Peradzynski, and Stamm (see Ref. 10).

[18]W. B. Hanson and J. R. Pellam, Phys. Rev. **95**, 321 (1954).

[19]M. J. Crooks and B. J. Robinson, Physica (Utrecht) **107B**, 339 (1981); Phys. Rev. B **27**, 5433 (1983).

[20]R. Mehrotra and G. Ahlers, Phys. Rev. B **30**, 5116 (1984); Phys Rev. Lett. **51**, 2116 (1983).

[21]D. S. Greywall and G. Ahlers, Phys. Rev. A **7**, 2145 (1973); Phys. Rev. Lett. **28**, 1251 (1972).

[22]T. Worthington, J. Yan, and J. U. Trefny, J. Low Temp. Phys. **24**, 365 (1976).

[23]T. Worthington, J. Yan, and J. U. Trefny, J. Low Temp. Phys. **22**, 293 (1976).

[24]G. Ahlers, in *Phase Transitions*, edited by M. Levy, J.-C. Le Guillou, and J. Zinn-Justin (Plenum, New York, 1982), p. 1.

[25]A. Singsaas and G. Ahlers, Phys. Rev. B **29**, 4951 (1984).

[26]Model DR-4S-4H, Microtech, Inc., 1420 Conchester Hwy., Boothwyn, PA 19061.

[27]Chromium on a tungsten wire, available from R. D. Mathis Co., 2840 Gurdy Ave., Long Beach, CA.

[28]L. Holland, *Vacuum Deposition of Thin Films* (Wiley, New York, 1956), Chap. 5.

[29]H. L. Caswell, Phys. Lett. **10**, 44 (1964).

[30]M. J. Crooks and B. J. Robinson, Rev. Sci. Instrum. **54**, 12 (1983).

[31]G. Laguna, Cryogenics **16**, 241 (1976).

[32]H. Borner, D. W. Schmidt, and W. J.Wagner, Cryogenics **19**, 89 (1979).

[33]For a review of lithographic procedures, see, for example, Sorab K. Ghandhi, *VLSI Fabrication Principles* (Wiley, New York, 1983), Chap. 10.

[34]See, for example, C. Kittel, *Elementary Statistical Physics* (Wiley, New York, 1958), Chap. 29.

[35]H. van Dijk, M. Durieux, J. R. Clement, and J. K. Logan, Natl. Bur. Stand. (U.S.) Monograph No. 10 (U.S. GPO, Washington, D.C., 1960).

[36]H. H. Sample and L. G. Rubin, Cryogenics **17**, 597 (1977).

[37]In this discussion the thermal mass of the bolometer and heater have been ignored. They are both sufficiently thin that the temperature of the surface of the glass substrate may be taken to be the heater-bolometer temperature.

[38]A. N. Tsoi and S. K. Nemirovskii, Fiz. Nizk. Temp. **6**, 671 (1980) [Sov. J. Low Temp. Phys. **6**, 324 (1980)].

[39]R. A. Fisher, G.E. Brodale, E. W. Hornung, and W. F. Giauque, Rev. Sci. Instrum. **39**, 108 (1968).

[40]Private communication from Corning Glass Works, Corning, NY 14830.

[41]L. D. Landau and E. M. Lifshitz, *Fluid Mechanics* (Pergamon, New York, 1959).

[42]Since the data points do not coincide for the two pulses, a cubic spline was used to interpolate between the points of the second pulse. Furthermore, the measured heater voltage indicated that the second pulse had a total power that was 1% larger than the first. Thus we multiplied the second pulse by

0.990 before fitting.

[43]R. Truell, C. Elbaum, and B. B. Chick, *Ultrasonic Methods in Solid State Physics* (Academic, New York, 1969), pp. 107–121.

[44]See, for example, W. H. Press, B. P. Flannery, S. A. Teukolsky, and W. T. Vetterling, *Numerical Recipes in C* (Cambridge University Press, Cambridge, England 1988), Chap. 17.

[45]G. Ahlers, in *The Physics of Liquid and Solid Helium,* edited by K. H. Bennemann and J. B. Ketterson (Wiley, New York, 1976), Pt. I, Chap. 2.

[46]S. Putterman and S. Garrett, J. Low Temp. Phys. **27**, 543 (1977)

[47]D. Marek, J. A. Lipa, and D. Philips, Phys. Rev. B **38**, 4465 (1988).